



UNIVERSITY OF LEEDS

This is a repository copy of *Extrinsic contributions to piezoelectric Rayleigh behavior in morphotropic PbTiO₃ - BiScO₃*.

White Rose Research Online URL for this paper:
<http://eprints.whiterose.ac.uk/119187/>

Version: Accepted Version

Article:

Tutuncu, G, Forrester, JS, Chen, J et al. (1 more author) (2017) Extrinsic contributions to piezoelectric Rayleigh behavior in morphotropic PbTiO₃ - BiScO₃. *Acta Materialia*, 137. pp. 45-53. ISSN 1359-6454

<https://doi.org/10.1016/j.actamat.2017.07.032>

© 2017 Acta Materialia Inc. Published by Elsevier Ltd. This manuscript version is made available under the CC-BY-NC-ND 4.0 license
<http://creativecommons.org/licenses/by-nc-nd/4.0/>

Reuse

Items deposited in White Rose Research Online are protected by copyright, with all rights reserved unless indicated otherwise. They may be downloaded and/or printed for private study, or other acts as permitted by national copyright laws. The publisher or other rights holders may allow further reproduction and re-use of the full text version. This is indicated by the licence information on the White Rose Research Online record for the item.

Takedown

If you consider content in White Rose Research Online to be in breach of UK law, please notify us by emailing eprints@whiterose.ac.uk including the URL of the record and the reason for the withdrawal request.

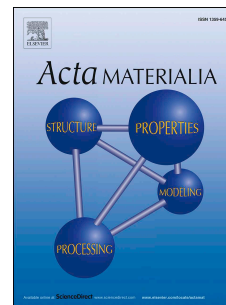


eprints@whiterose.ac.uk
<https://eprints.whiterose.ac.uk/>

Accepted Manuscript

Extrinsic contributions to piezoelectric Rayleigh behavior in morphotropic PbTiO_3 - BiScO_3

G. Tutuncu, J.S. Forrester, J. Chen, J.L. Jones



PII: S1359-6454(17)30593-1

DOI: [10.1016/j.actamat.2017.07.032](https://doi.org/10.1016/j.actamat.2017.07.032)

Reference: AM 13931

To appear in: *Acta Materialia*

Received Date: 6 April 2017

Revised Date: 11 July 2017

Accepted Date: 14 July 2017

Please cite this article as: G. Tutuncu, J.S. Forrester, J. Chen, J.L. Jones, Extrinsic contributions to piezoelectric Rayleigh behavior in morphotropic PbTiO_3 - BiScO_3 , *Acta Materialia* (2017), doi: [10.1016/j.actamat.2017.07.032](https://doi.org/10.1016/j.actamat.2017.07.032).

This is a PDF file of an unedited manuscript that has been accepted for publication. As a service to our customers we are providing this early version of the manuscript. The manuscript will undergo copyediting, typesetting, and review of the resulting proof before it is published in its final form. Please note that during the production process errors may be discovered which could affect the content, and all legal disclaimers that apply to the journal pertain.

Extrinsic contributions to piezoelectric Rayleigh behavior in morphotropic PbTiO_3 - BiScO_3

G. Tutuncu,¹ J. S. Forrester,² J. Chen,³ and J. L. Jones^{1*}

¹*Department of Materials Science and Engineering, North Carolina State University, Raleigh, NC 27695, USA*

²*School of Chemical and Process Engineering, University of Leeds, Leeds, West Yorkshire, LS2 9JT, UK*

³*Department of Physical Chemistry, University of Science and Technology Beijing, Beijing 100083, China*

In situ, high-energy, time-resolved X-ray diffraction experiments are utilized to quantify contributions from non-180° domain wall motion to the macroscopic electromechanical coupling effect in the morphotropic phase boundary composition 0.64PbTiO_3 - 0.36BiScO_3 during the application of weak electric field amplitudes. Macroscopic piezoelectric coefficient measurements are compared with diffraction data. The results demonstrate a linear contribution of electric-field-amplitude-dependent non-180° domain wall motion at small field amplitudes, and therefore domain wall motion contributes directly to the Rayleigh behavior of piezoelectric coefficients.

Keywords: Domain wall motion; Rayleigh behavior; high-energy synchrotron radiation; morphotropic piezoelectrics

* Corresponding Author: email jacobjones@ncsu.edu, Tel: +1-919-575-4557

1. Introduction

Solid solutions of two (or more) ferroelectric phases often exhibit improved dielectric, piezoelectric properties, and strong electromechanical coupling near the morphotropic phase boundary (MPB) region. An MPB is a compositionally configured region separating the components of the solid solution with different orientations of polarization. Among these compositions, $x\text{PbTiO}_3 - (1-x)\text{BiScO}_3$ (PT-BS) is a binary system that has received attention due to the elevated piezoelectric properties at/near the MPB region. The phase diagram of PT-BS suggests that when $x = 0.64$ (0.64PT-0.36BS) the composition is in the vicinity of the MPB region, with coexisting tetragonal and either rhombohedral or monoclinic phases, and showing a high piezoelectric response ($d_{33} \cong 460$ pC/N) [1-6].

The dielectric and electromechanical properties of piezoelectric ceramics are known to be largely affected by multiple unique physical mechanisms. The intrinsic effects, associated with contributions from the crystal lattice, include polarization vector rotation between miniaturized domains of the crystal symmetries coexisting at the MPB, and lattice distortion under an external stimulus. Recently, a systematic study by Liu et al. [7] has demonstrated that the type of electric-field-induced polarization rotation in the monoclinic phase plays an important role in the high piezoelectric properties. On the other hand, extrinsic contributions are shown to be mainly due to domain wall motion [8-15]. It has also been suggested that the presence of low symmetry structures enhance either the intrinsic (by flattening the free energy profile) [16] or extrinsic (by enabling higher domain wall motion) [17] material responses.

In ferroelectric ceramics, the irreversible extrinsic (non-lattice) contributions, including domain wall motion, to material properties such as the piezoelectric coefficients, can be significant and inferred from field-amplitude-dependent measurement of the converse piezoelectric effect.

Under an electric field, ferroelectric domain walls and/or phase boundary motion can displace between (reversible), and also across (irreversible) randomly distributed pinning centers such as defects and grain boundaries, and contribute to the hysteresis and nonlinearity. For a material with randomly distributed pinning centers, the relationship between the piezoelectric coefficient and low-to-mid range electric field amplitudes can then be described by the Rayleigh law, and is given as [18-21]

$$d_{33} = d_0 + \alpha E \quad (1)$$

where d_{33} is the converse longitudinal piezoelectric coefficient in reduced form [22], d_0 is the value of d_{33} extrapolated to zero electric field amplitude, $E = 0$ and α (the slope of d_{33} against E_0) is the Rayleigh coefficient of linear increase in d_{33} with E . Eqn. (1) may contain higher order terms if the average energy landscape surrounding domain walls in a material is not with random potentials, i.e. domain wall motion is not random. Both parameters d_0 and α are strongly related to the microstructure and crystal structure of the materials of interest [23]. While d_0 includes contributions from both the intrinsic piezoelectric effect and reversible displacement of interfaces (e.g., domain wall motion or phase boundary motion) α represents contributions from the irreversible displacement of interfaces.

Rayleigh law has been widely used to describe the piezoelectric, dielectric and ferroelectric properties of bulk ceramics [9,19,20,23-26]. In the present work, the converse piezoelectric coefficients are analyzed in the context of Rayleigh law to assess and deconvolute the extrinsic contributions, e.g., domain wall motion, to the overall piezoelectric response as a function of applied electric fields to the MPB composition 0.64PT-0.36BS. Stroboscopic time-resolved X-ray diffraction (XRD) techniques are utilized to characterize the displacement of domain walls over local energy barriers using the changes in the relative intensities of characteristic reflections under

cyclic, weak electric field amplitudes. In the case of tetragonal perovskite ferroelectrics, the volume fraction changes of ferroelastic, or non-180°, domains can be quantified by tracking the changes in the relative intensities of diffraction line profiles with ferroelectric distortion parallel to the [001] crystallographic axis.

2. Experimental procedure

Solid state synthesis was used to prepare samples of 0.64PT-0.36BS. The starting powders of $\text{Pb}(\text{CO}_3)$, Bi_2O_3 , TiO_2 and Sc_2O_3 were stoichiometrically mixed and ball milled in ethanol for 12 h. After drying, the mixture was calcined at 760 °C for 5 h and ball milled for an additional 12 h. The calcined powder was then pressed into disk-shaped pellets and sintered in a closed crucible at 1100 °C for 1 h embedded in calcined powder of the same composition. An XRD pattern of the as-synthesized material confirmed the phase purity and coexistence of a tetragonal phase with a second polymorph, which is attributed to either a rhombohedral or monoclinic phase as stated in prior observations [1-6]. The grain size of the samples was approximately 1 μm from scanning electron microscope micrographs using a linear intercept method.

The pellets were polished using 1 μm diamond paste on diamond lapping films, and silver electrodes were applied onto the top and bottom surfaces, the samples were then fired at 550 °C for 30 min. Polarization and strain loops were measured on initially unpoled materials at field amplitudes of 8 kV/mm using triangular wave forms and a frequency of 10 Hz. Samples were then poled at 100 °C for 10 min with a constant electric field amplitude of 4 kV/mm. The direct longitudinal piezoelectric coefficient was measured on multiple locations of multiple samples using a Berlincourt d_{33} meter (ZJ-6A, CAS). The measurements of strain responses of the poled samples were repeated under bipolar field amplitudes varying below and near the coercive field. In

these measurements, an electric field was applied using a sinusoidal waveform with the frequency of 0.3 Hz and the material response was recorded on a ferroelectric analyzer (TF1000, aixACCT, Germany).

The samples for *in situ* diffraction experiments were prepared by cutting into dimensions of 1 mm x 1.08 mm x 5 mm, and after polishing they were annealed at 650 °C for 3 h to eliminate residual stress from the cutting process and ensure a depoled state. Gold electrodes were sputter coated to 1 mm x 5 mm parallel surfaces of the sample and a topcoat was applied using a commercial conductive silver paint prior the electric field application. High-energy synchrotron XRD experiments using a wavelength of 0.107980 Å (114 keV) were conducted on beamline 11-ID-C at the Advanced Photon Source, Argonne National Laboratory. A beam size of 500 μm x 500 μm was incident on the material corresponding to a sampled volume of approximately 0.27 mm³ (or equivalently ~3 x 10⁷ grains) for each measurement. The sample was placed in a custom-made sample holder [27], and immersed in dielectric fluid inside a Kapton load cell to avoid arcing during electric field application. The electric field was applied perpendicular to the beam direction using a high voltage amplifier (Matsusada model COR-10B2). Diffraction patterns were measured in forward scattering geometry (transmission mode) on a Perkin-Elmer amorphous silicon area detector placed at approximately 1800 mm from the sample stage.

The two-dimensional diffracted intensities are integrated over azimuthal sectors with 15° widths, yielding orientation-dependent information on the material response. Using this configuration, the scattering intensities measured in the vertical direction of the 2D detector are oriented within ±7.5° to the applied electric field direction. In this geometry, enabled by the high-energy setup and resultant small scattering angles (2θ), the misorientation angle between the scattering vector on the detector and the electric field direction in the present work is $2\theta/2 \approx 1.5^\circ$

and $\approx 1.3^\circ$ for 002 and 111 reflections, respectively. Therefore, the plane normal being measured is considered approximately parallel to the direction of the applied electric field in the vertical direction of the detector, $\varphi = 0^\circ$ (equivalently in the horizontal direction, $\varphi = \pi/2$ represents the sample response perpendicular to the electric field direction) [4-14, 28]. Due to the symmetric nature of the diffraction data, any of the four quadrants of sample directions of a poled polycrystalline ceramic ideally should yield equivalent results. Therefore, only the first quadrant, $0 \leq \varphi \leq \pi/2$ of the data is presented in this work.

An XRD pattern was first measured for the unpoled state of the sample as a reference pattern. Then the measurements were carried out for 1s during poling measurements under a bipolar electric field using a triangular wave function and a frequency of 0.0125 Hz. Prior to subcoercive stroboscopic measurements, the sample was subjected to 3.6 kV/mm constant electric field amplitude for 5 min to increase the strength of the poling process. The samples were then subjected to cyclic electric fields of a square wave form with a frequency of 0.33 Hz at varying amplitudes from ± 500 V/mm to ± 2250 V/mm to obtain time-resolved stroboscopic measurements. For the stroboscopic measurements, the electric field was synchronized with the detector electronics. To increase the total observed intensities, data over 50 cycles were summed for positive and negative electric field signals separately. Diffraction intensities as a function of 2θ were then modeled in Matlab (MathWorks, R2012a) to appropriate profile shape functions, such as Gaussian or Pearson-VII type peak profiles, and integrated peak intensities and positions were extracted. Error bars were calculated through error propagation from the parameters obtained within a 95% confidence level of the profile fitting procedure.

Crystal structure refinement of the diffraction data prior to the electrical poling cycle of the 0.64PT-0.36BS sample was carried out using the Rietveld refinement program GSAS [29]. The

background was modeled using the Chebyshev model, varying 12 parameters. A mixed-phase refinement using the tetragonal space group $P4mm$ and the monoclinic space group Cm was used to model the data, similar to that used in Refs. 4-6. Since Pb and Bi share the same site, the atomic position and displacement parameters were constrained as equal, the total site occupancy was set as fully occupied, and they were refined opposite each other. The same constraints were used for Sc and Ti atoms. The peak shape parameters for two phases were set as equal using function type 4. The 2θ zero offset, scale factor, lattice parameters, atomic positions, isotropic atomic displacement parameters (with the exception of oxygen atoms), and atomic site occupancy parameters were first refined independently and then concurrently. A similar procedure was adopted for the poled states of the sample, using additional preferred orientation parameters. For simplicity, the reflections are labeled according to their pseudo-cubic (PC) indices.

3. Results and Discussion

The ferroelectric composition 0.64PT-0.36BS is a well-known ferroelectric material with known properties. Nevertheless, it is prudent to quantitatively measure the piezoelectric properties of the samples studied herein. To this end, the direct piezoelectric coefficient was measured as 461 pC/N, which is similar to the previously reported values within a standard deviation of ± 11 pC/N. Further details of the property measurements are given in Refs. 11 and 12. In brief, the coercive field was determined as 2.2 kV/mm from the polarization and strain measurements in response to bipolar electric field amplitudes at ± 5 kV/mm. The remanent polarization, P_r , after the electric field is removed is $44 \mu\text{C}/\text{cm}^2$, while the peak-to-peak strain measured is 0.58%. After poling, cyclic electric fields were applied to the sample with progressively increasing amplitudes up to 2.25 kV/mm, in close proximity to the ferroelectric coercive field. The strain measurements are

shown in Fig. 1 (two measurements above 1.85kV/mm are omitted in Fig.1 for clarity), in which the strain values that the material exhibits increase with field amplitudes, more pronounced in the vicinity of the coercive field.

Figure 2 (a) and (b) illustrates the XRD patterns ($\varphi = 0^\circ$) in the region of the $\{111\}_{\text{PC}}$ and $\{002\}_{\text{PC}}$ (where PC refers to the pseudo-cubic cell setting) during the application of a bipolar electric field with the amplitudes above the coercive field, E_c . In Fig. 2(c), $E_c \approx \pm 2$ kV/mm values are added to aid in the interpretation of the diffraction pattern. There are significant intensity changes within the $\{002\}_{\text{PC}}$ diffraction profile, accompanied by a change in the average 111 interplanar spacing. These changes are more apparent in Fig. 2(d), in which XRD patterns are compared at two representative electric field amplitudes, 0 and 3.6 kV/mm. The changes in intensities are attributed to domain switching under the influence of an electric field [8-15]. Initial observation of the additional Bragg scattering between the tetragonal 002_{T} and 200_{T} reflections, at lowest and highest 2θ positions, may suggest that this intensity is related to the existence of 002 and 220 reflections of a monoclinic phase [3]. However, as seen in Fig. 2(b), within the resolution of this study, monoclinic 002_{M} and 220_{M} reflections are not easily resolved. This is due to overlap from the tetragonal 002_{T} and 200_{T} reflections and diffuse scattering, which manifests itself in the diffraction pattern as a broadening effect causing the increased intensity in the overlap region [28]. Therefore, these additional reflections are treated as a single profile for further analysis in the present work.

In the tetragonal phase, the degree of orientation, f in terms of multiples of random distribution (m.r.d.) may be calculated using changes in the intensities of the tetragonal 200_{T} and 002_{T} reflections relative to the intensities in an initially unpoled sample [8, 30]

$$f_{002}(m.r.d.) = 3 * \frac{\frac{I_{002}}{I'_{002}}}{\frac{I_{002}}{I'_{002}} + 2 \left(\frac{I_{200}}{I'_{200}} \right)} \quad (2)$$

where I_{hkl} is the integrated intensity of the hkl reflection for a given sample in the presence of electric field. I'_{hkl} is the integrated intensity of the same reflection prior to the application of electric field. With no preferred orientation in the material, it can also be represented in unitless form as the volume fraction of electric-field-induced domain reorientation, η_{002}

$$\eta_{002} = \frac{f_{002}}{3} - \frac{1}{3} \quad (3)$$

The integrated intensity and 2θ positions were extracted by fitting the measured intensity profile of $\{002\}_{PC}$ region to three Gaussian profile shape functions. These three peaks represent tetragonal 002 and 200 reflections and a region representing the unresolved monoclinic reflection. During peak fitting, the widths of all three peaks were constrained as equal, under the assumption that there are only infinitesimal variations in microstructural contributions, i.e. domain size etc. of these two phases.

The domain volume fraction for the tetragonal phase calculated using Eqns. (2) and (3) are given in Fig. 3 as a function of electric field amplitude and representative orientations relative to the field direction. In polycrystalline ferroelectrics, the maximum allowable fraction of the switched domains under electric field is 0.67 for the tetragonal phase [8, 30]. However, in practical applications, due to the intergranular mechanical constraints imposed from neighboring grains, this value is not attained. Here, 0.64PT-0.36BS exhibits a relatively high value, $\eta_{002} = 0.57$ (Fig. 3) indicating a high degree of domain re-alignment after the poling.

The characteristic degenerate reflections in the monoclinic phase are not easily distinguished from each other within the resolution of the current study. Thus, a description

equivalent to Eq. (3) may lead to erroneous interpretations of the extent of domain wall motion in the monoclinic phase. It was previously demonstrated that the 111 peak shift can be used as a strain monitor in tetragonal materials because {111} planes do not exhibit domain switching [31, 32]. In polycrystalline materials, there are several competing electric-field-induced strain mechanisms, i.e. the strain attributed to domain wall motion, electric-field-induced lattice strain from piezoelectricity, and the elastic intergranular strain. It has been suggested that in “extender” ferroelectrics, the piezoelectric response will be maximized when the electric field direction is parallel to the polar direction in the crystal due to extension of the polar vector (in *hhh* rhombohedral and *00h* planes in tetragonal crystals) [33, 34] rather than polarization rotation. Thus, grains with more domain wall motion can impose constraints on neighboring grains. In the tetragonal phase, {111} planes are then subjected to large tensile stress to accommodate these intergranular interactions due to domain switching in neighboring domains and/or grains [8, 35] in addition to the intrinsic piezoelectric strains. Similarly, in rhombohedral compositions, ferroelastic domain wall motion induces strain in {002} orientations. Moreover, in the monoclinic phase, domain wall motion would also result in intensity redistribution between ferroelastic peaks contributing to the {111}_{PC} diffraction profile. However, the {111}_{PC} diffraction profile observed here is not visibly split into multiple contributing reflections of monoclinic 201_{PC,M} and 021_{PC,M} reflections and exhibits only a slight asymmetric broadening. This interaction between domain switching and lattice strain along the crystallographic directions affects the strain values. The electric-field-induced strain in 111 then suggests a complicated stress-strain state in this structurally inhomogeneous MPB material and cannot be completely attributed to the piezoelectric effect. Therefore, it is concluded that a shift in the {111}_{PC} position may not originate exclusively from the piezoelectric response of the crystal but may also be contributed by the effects of

ferroelastic domain wall motion (changing intensities between monoclinic $201_{PC,M}$ and $021_{PC,M}$ reflections) [12] and would relate to the extent of domain switching in the monoclinic phase.

In this study, the measured shift towards a lower 2θ value corresponds to $\sim 0.5\%$ strain (Fig. 4). This value is $\sim 0.15\%$ for subcoercive field amplitudes (~ 1.9 kV/mm). The onset of domain switching in the tetragonal phase and drastic changes in the 111 strain coincides with the coercive field of this material, suggesting that domain switching in both phases is interrelated. Similarly, the representative changes of domain fractions in rhombohedral and tetragonal phases in PT-0.3725BS pinpoint no significant variation for the onset of domain switching in both phases [5].

The effect on the relative intensities of monoclinic $201_{PC,M}$ and $021_{PC,M}$ profiles (which contribute to the 111 peak profile) due to electric-field-induced domain wall movement in the monoclinic phase at amplitudes below the coercive field may also be estimated from the systematic changes in the full width at half maximum (FWHM) of the $\{111\}_{PC}$ profile. Figure S1 (Supplementary Information) shows the change in FWHM of the $\{111\}_{PC}$ diffraction profile for a field amplitude of 1.5 kV/mm during the positive and negative polarity of the waveform. The difference in the profile width between positive and negative polarity is outside the error bars and approximately 0.00076° at 1.5 kV/mm and this value slightly increases with increasing field amplitude up to 0.00085° at 1.9 kV/mm. It has been demonstrated that the difference in the FWHM between positive and negative polarities is also frequency dependent, further evidence of an extrinsic origin of this response due to domain wall motion in the monoclinic phase [12].

Additional insight into domain switching in the monoclinic phase is provided from the lattice strain coefficients. The peak to peak electric field induced strain coefficients are obtained from the relative shift in the diffraction profiles between the positive and negative polarity of the

electric field $(d_{hkl,positive} - d_{hkl,negative})/d_{hkl,negative}$ divided by the electric field amplitude, $\pm E$. $d_{hkl,positive}$ and $d_{hkl,negative}$ represent the lattice spacings at the maximum and negative electric fields, respectively, for the cyclic electric field. The resultant values are shown in Fig. S2. While the strain coefficient for the tetragonal 002_T reflection changes from $200 (\pm 26)$ pm/V to $970 (\pm 28)$ pm/V with increasing field amplitude from 0.5 to ~ 1.9 kV/mm, the strain coefficient for the tetragonal 200_T is indistinguishable from 0 pm/V. This is consistent with the behavior of an extender ferroelectric, where the maximized strain is parallel to the polarization direction [33,34]. Calculation of an effective strain coefficient for the monoclinic phase using the 002_M profile, on the other hand, yields values ranging from $490 (\pm 35)$ pm/V to $1250 (\pm 68)$ pm/V and thus providing a stronger contribution to the overall material properties. It should be noted, however, that the monoclinic 002_M profile is comprised of 002_M and 220_M reflections. Due to the fact that these two planes are not clearly resolved from each other, the effective strain coefficient for the monoclinic 002_M profile is an average value of two reflections and the strain values could represent the piezoelectric effect and/or domain wall motion in the monoclinic phase. Since the strain coefficients for the monoclinic phase are also frequency dependent unlike the tetragonal phase (as presented in Ref. 12), the domain wall motion in the monoclinic phase is a more likely basis for these values rather than intrinsic piezoelectric effect of the crystalline lattice. Thus, the intensity redistribution due to domain wall movement can be then observed as an overall shift in the position of 002_M peak.

A representative measurement containing pseudocubic 002-type reflections during the positive and negative polarity of subcoercive electric field measurements is shown in Fig. 5 for 1.5 kV/mm. The intensity interchanges between the 002_T and 200_T reflections under positive and negative polarity of the applied field are outside the calculated error bars and they are correlated to non- 180° domain switching at weak alternating electric field amplitudes. Domain wall motion in

the tetragonal phase can simply be demonstrated by the intensity ratio of 002_T and 200_T reflections. Figure S3 shows such a representation for 1.5 kV/mm, with a higher intensity ratio for positive polarity compared to the negative polarity due to an increase in the volume fraction induced by electric field during positive polarity.

As mentioned above, the monoclinic distortions are not easily visible within the current resolution. Nevertheless, previous studies [4-6] have demonstrated a best fit to diffraction patterns of similar compositions using two-phase model with tetragonal ($P4mm$) and monoclinic (Cm) phases. Thus, the crystal structure of the present sample was determined from the Rietveld refinement using a combination of these two phases. Figure S4 shows the calculated and measured diffraction patterns for the sample prior to applying electric field. The refinement outputs and quality of fit indicators are listed in Table S1 for both the unpoled and the sample poled at 3.6 kV/mm along the applied field direction. The refinement results indicate that upon poling, the fraction of tetragonal phase increases from $\sim 33\%$ to 38.4% at the expense of the monoclinic phase. This is different than what was observed in the morphotropic $\text{Pb}(\text{Zr}_{0.535}\text{Ti}_{0.465})\text{O}_3$, where tetragonal phase completely transforms into the monoclinic phase under the electric field exhibiting large lattice strains [36]. Khatua et al. [4,5] and Lalitha et al. [6] reported that when compared to a single phase rhombohedral composition of the same material, there is a decrease in the domain wall motion in the rhombohedral phase in the MPB composition PT-0.3725BS during poling above coercive field amplitudes. It was concluded that the field-induced transformation from monoclinic to tetragonal phase was the most significant factor for the large piezoelectric response in the MPB composition, while the contribution from the domain switching in the rhombohedral phase was relatively higher than that in the tetragonal phase.

In the present work, to aid in the interpretation of the implications of the phase changes during the application of alternating, subcoercive electric field amplitudes, the phase fractions

were extracted from the Rietveld refinements of patterns in parallel to the electric field. The maximum increase in the tetragonal phase fraction observed was $\sim 1.12(3)\%$ when switching from positive to negative polarity below the coercive field (~ 1.9 kV/mm). Additionally, to further examine the change in the monoclinic and tetragonal phase fractions between positive and negative polarity, the ratio of the monoclinic $\{002\}$ intensity to the total tetragonal intensity (the sum of the tetragonal 002_T and 200_T integrated intensities) is used. Due to substantial domain wall movement, changes in the fraction of certain crystal orientations will produce discrepancies in the observed intensity of hkl reflections with respect to a powder average in which grain orientations are completely random. These systematic distortions in reflection intensities can be modeled with functions having coefficients, which are adjusted during crystal-structure refinement. However, the results of a Rietveld refinement are most reliable when the diffraction patterns are recorded using randomly oriented crystallites. Therefore, employing the ratio of the monoclinic intensity to the total tetragonal intensity should provide a superior result that is more straightforward to calculate. The resulting values are shown in Fig. S5 and demonstrate small changes up to 2 kV/mm. The effects of an electric-field-induced phase transition between the two phases (Fig. S5) are an order of magnitude lower at these field amplitudes compared to domain wall motion in the tetragonal phase (Fig. S3). With increasing field amplitudes above ~ 1.8 kV/mm (Fig. S5), the ratio between the two phases slightly decrease and exhibits a discrepancy between the positive and negative polarity ($\sim 2\%$) in accordance with the structural refinements presented above. In addition, it has been recently demonstrated that below the coercive field, the extent of interphase boundary motion between coexisting monoclinic and tetragonal phases is not as clearly frequency dependent as domain wall motion in the tetragonal phase, indicating a weak contribution to the frequency dispersion of the piezoelectric coefficient, i.e. the extrinsic origin of the material property [12]. In conclusion, the present results reveal that interphase boundary motion, as measured through

changes in phase fractions of coexisting tetragonal and monoclinic phases, must play a very minor role in the piezoelectric properties of 0.64PT-0.36BS.

Using the peak fitting procedure represented in Fig. 2, changes in the domain wall fractions in the tetragonal phase during the positive and negative polarity are calculated by

$$\Delta\eta_{002} = \eta_{002}^{+} - \eta_{002}^{-} \quad (4)$$

where η_{002}^{+} and η_{002}^{-} are values of η for maximum positive and minimum negative electric fields relative to the unpoled state, respectively. A change in preferred domain orientation is calculated from XRD patterns using Eqns. (3) and (4) at all angles with respect to the electric field direction due to the fact that domain wall motion in all orientations contributes to the averaged polycrystalline material response. After electric field application, the volume fraction of the domains with [002] parallel to the electric field direction increases and the opposite is seen for the perpendicular direction. Figure 6 shows $\Delta\eta_{002}$ as a function of field amplitude as well as orientation with respect to the direction of applied field. It can be observed that $\Delta\eta_{002}$ decreases as the sample orientation is away from the electric field direction, becoming negative for angles above $\sim 45^{\circ}$. With increasing electric field amplitude, the volume fraction of the domains, $\Delta\eta_{002}$ increases with values reaching 10% near the coercive field amplitude for directions parallel to the electric field direction.

The relative contribution of non- 180° domain wall motion to macroscopic longitudinal strain of the sample can be quantified by utilizing the information obtained from Eqn. (3). Non- 180° reorientation creates spontaneous strain, S , in the crystal lattice, which is associated with $(d_{00h}-d_{h00}) / d_{h00}$ or as a function of lattice parameters, $(c/a)-1$ for tetragonal crystals. In this study, the value of S is calculated from the unpoled sample for simplicity since the changes in the lattice during the electric field application do not impact the absolute final values beyond 0.2%. Then, the

macroscopic strain due to all non-180° domain wall motion within a polycrystalline material can be obtained using a weighted summation of strains in the entire three-dimensional crystallographic orientation space with respect to the electric field direction $0 \leq \varphi \leq \pi/2$, and is given by [8,30]:

$$\langle \varepsilon_{non-180^\circ} \rangle = S \int_{\varphi=0}^{\varphi=\pi/2} [m \Delta \eta_{002}(\varphi) \cos^2 \varphi] \sin \varphi d\varphi \quad (5)$$

where $m=3$ for tetragonal ceramics. While $m \Delta \eta_{002}$ corresponds to the field-induced change in the distribution of domain variants, the geometric factors $\sin \varphi$ and $\cos^2 \varphi$ describe the transformation between the sampling volume and orientation space due to domain wall motion in the direction of the electric field.

The macroscopic strain due to microscopic non-180° domain motion is calculated using Eqn. (4) at various electric field amplitudes and the strain coefficient due to non-180° domain wall motion at each field amplitude is given by:

$$d_{33 non-180^\circ} = \frac{\langle \varepsilon_{non-180^\circ} \rangle}{2E} \quad (6)$$

This representation has been previously applied for single phase Pb(Zr,Ti)O₃-based materials [10,37] to represent electric field-induced strain coefficients due to domain wall motion. It is emphasized that these strains are due to electric-field-induced domain wall motion and not to be confused with the intrinsic piezoelectric effect.

For a direct evaluation of the contribution of non-180° domain wall motion to macroscopic nonlinearity in the piezoelectric property, the strain coefficient calculated from the diffraction data in Eqn. (5) can be compared with the piezoelectric coefficient measured macroscopically. To accomplish this, the macroscopic field-induced strain (Fig. 1) was used to calculate the converse longitudinal piezoelectric coefficient, d_{33} .

The longitudinal strain response to the electric field is related to the longitudinal converse piezoelectric coefficient d_{33} . This coefficient is theoretically equivalent to the direct piezoelectric coefficient and is described by the relationship between mechanical strain parallel to the poling direction and electric field amplitude:

$$d_{33} = (\epsilon_{\max} - \epsilon_{\min}) / 2E \quad (7)$$

where E is the applied field signal and $\epsilon_{\max} - \epsilon_{\min}$ is the peak-to-peak strain amplitude. These measurements of strain response were carried out with incremental steps of electric field amplitudes using a sine wave electric field. The corresponding d_{33} values were then compared with $d_{33, non-180^\circ}$ where the coefficient is calculated from the diffraction data during application of a square-wave electric field. Although the two different types of measurements utilized different waveforms of the same frequency, the nature of electric field waveforms is not expected to have a significant impact on the data interpretation as described in Ref. 9.

Figure 7 shows the d_{33} and $d_{33, non-180^\circ}$ values for all field amplitudes. As expected, due to other possible contributions to the macroscopic electric-field-induced strain in addition to non-180° domain wall motion, the values of $d_{33, non-180^\circ}$ are smaller than d_{33} throughout the applied electric field amplitude range. The behavior in Fig. 7 can be considered within three distinct regions. The weak field region, below 1 kV/mm demonstrates negligible domain wall contributions from the tetragonal phase. It has been shown that below 1 kV/mm, deaging [11, 38, 39], i.e., progressive loss in non-180° domain wall alignment as an irreversible change occurs during initial cycling under weak fields.

For the intermediate electric field amplitudes ranging from 1 to ~ 2 kV/mm, the data are consistent with a Rayleigh-like behavior, wherein $d_{33, non-180^\circ}$ increases linearly with field

amplitudes. Thus, the values of $d_{33, non-180^\circ}$ were fit using a linear regression similar to Eqn. (1) within this regime using the following:

$$d_{33, non-180^\circ} = d_{33, non-180^\circ}^0 + \alpha_{non-180^\circ} E_0 \quad (8)$$

where $d_{33, non-180^\circ}^0$ is the field-independent contribution of non-180° domain walls (the reversible contribution) while the field-dependent behavior is characterized by $\alpha_{non-180^\circ}$ [9]. The resulting fit values for d_{33} and $d_{33, non-180^\circ}$ are reported in Fig. 7. In the higher electric field region with amplitudes greater than 2 kV/mm, a relatively larger increment in the slope of $d_{33, non-180^\circ}$ is observed and this defines the upper limit of the Rayleigh region for this material [10].

The Rayleigh parameters α and d_0 obtained from the linear fit of Eqn. (1) to macroscopic measurements of piezoelectric response can contain contributions from the intrinsic piezoelectric effect, interphase boundary motion and reversible or irreversible domain wall motion. On the other hand, the values extracted from the $d_{33, non-180^\circ}$ data represent exclusively non-180° domain wall motion contributions to the piezoelectric coefficient. For example, $d_{33, non-180^\circ}$ represents solely the reversible contribution of non-180° domain wall motion to the piezoelectric coefficient and the value is smaller than the d_0 value obtained through a Rayleigh fit to the macroscopic measurement, since d_0 represents all possible reversible displacement of interfaces and the intrinsic piezoelectric effect of the lattice.

It is noted that the α and $\alpha_{non-180^\circ}$ values obtained for 0.64PT-0.36BS are close ($\pm 1\%$ difference), suggesting a similar nonlinearity between the macroscopic electric field-induced piezoelectric strains and the strains due to non-180° domain wall motion. This observation directly demonstrates that non-180° domain wall motion in the tetragonal phase provides the dominant contribution to the Rayleigh behavior of the converse piezoelectric coefficient in this material.

The overall contribution of non-180° domain wall motion to piezoelectric nonlinearity in the

present material can be compared to those measured previously using similar methods, for example $\text{Pb}(\text{Zr},\text{Ti})\text{O}_3$ -based materials. For a 2 at% La-doped $\text{PbZr}_{0.52}\text{Ti}_{0.48}\text{O}_3$ single-phase material, the contribution of non- 180° domain wall motion to the converse d_{33} coefficients reached ~45% at the highest field amplitudes [10]. For a commercial $\text{Pb}(\text{Zr},\text{Ti})\text{O}_3$ -based single-phase material, the relative contribution was 34% [37]. In contrast, the present work on the tetragonal phase of 0.64PT-0.36BS is lower with relative contributions maximizing at ~20% at the highest field amplitudes. For this PT-BS composition, these results suggest that additional cooperating mechanisms contribute to the converse piezoelectric coefficient, e.g., domain wall motion in the second, co-existing polymorph phase (of monoclinic symmetry) and/or field-induced phase transformation. In related work, Khatua et al. [4] reported that although the magnitudes of the changes are very small, the volume fraction and domain reorientation of the rhombohedral phase in MPB PT-0.3725BS are correlated under low field electric field. Based on the results of the present work, the change in phase fraction of the tetragonal phase shows distinguishable but small values (1%) under low field amplitudes in 0.64PT-0.36BS. A precise calculation of the contribution of the domain wall motion in the monoclinic phase to the macroscopic properties was not readily available due to the overlapping reflections of the subtly distorted monoclinic crystal. Nevertheless, evidence (Figures S1 and S2) suggests that the monoclinic phase has substantial domain wall motion occurring.

Overall, an extensive investigation of structural changes in the subcoercive field regime is presented. Complementing the prior work [4-6], a manifold correlation between the lattice strain and field-induced domain switching in both monoclinic and tetragonal phases is observed at these field amplitudes. In Ref. [12], it was shown that 0.64PT-0.36BS exhibits extensive domain wall motion in the monoclinic phase and this provides a major contribution to the electric-field-induced strain and piezoelectric coefficient of 0.64PT-0.36BS. It is therefore concluded that the high

converse piezoelectric coefficients of 0.64PT-0.36BS are collectively contributed from domain wall motion in both the tetragonal and monoclinic phases at field amplitudes below coercive field, accompanied with weak, but measurable contributions from the electric-field-induced phase transitions at these field amplitudes. It should be emphasized that each material system and their MPB can exhibit different and complicated characteristics based on the composition and type of the coexisting phases. The time-resolved XRD technique and methodology employed here [10-12] could be used to better understand the correlations among the intrinsic and extrinsic contributions to the macroscopic properties in other compositions and materials.

Conclusions

It is demonstrated that the PT-BS MPB composition examined here follows a Rayleigh-like behavior under weak field electric field amplitudes. The method used enables the direct evaluation of the non-180° domain wall motion contribution to the piezoelectric Rayleigh behavior. Using synchrotron-based X-ray diffraction, changes in the volume fractions of non-180° domains during the application of cyclic electric fields below the coercive field were measured. Domain wall motion was quantified in the tetragonal phase by a change in the relative intensities of the 002_T and 200_T reflections and the converse longitudinal piezoelectric coefficient is calculated from field-amplitude-dependent strain measurements of the material. While the Rayleigh variables extracted from the macroscopic measurements describe all extrinsic contributions to the piezoelectric coefficient, diffraction measurements provided a direct quantification of the non-180° domain wall motion contribution. A direct comparison between the strain coefficient due to non-180° domain wall motion in the tetragonal phase and converse longitudinal piezoelectric

coefficient suggests the nonlinearity in the macroscopic electromechanical response of the material mainly stems from non-180° domain wall motion.

Acknowledgments

JJ and GT acknowledge support from the U.S. Department of the Army under W911NF-09-1-0435, and JC from the National Natural Science Foundation of China (Grants 91022016, 21322102 and 21031005). Use of the APS was supported by the U.S. Department of Energy, Office of Science, Office of Basic Energy Sciences, under Contract No. DE-AC02-06CH11357. The authors gratefully acknowledge Yang Ren and Guy Jennings for assistance with the XRD measurements.

References

- [1] R. Eitel, C.A. Randall, T.R. Shrout, P.W. Rehrig, W. Hackenberger, S.-E. Park, New high temperature morphotropic phase boundary piezoelectrics based on Bi(Me)O₃-PbTiO₃ ceramics, *Jpn. J. Appl. Phys. Part 1* 40 (2001) 5999.
- [2] R. Eitel, C.A. Randall, T.R. Shrout, S.-E. Park, Preparation and characterization of high temperature perovskite ferroelectrics in the solid-solution (1-x)BiScO₃-xPbTiO₃, *Jpn. J. Appl. Phys. Part 1* 41 (2002) 2099.
- [3] B. Kim, P. Tong, D. Kwon, J.M.S. Park, B.G. Kim, Temperature-dependent neutron diffraction study of phase separation at morphotropic phase boundary in (1-x)BiScO₃-xPbTiO₃, *J. Appl. Phys.* 105 (2009) 114101.
- [4] D.K. Khatua, K.V. Lalitha, C.M. Fancher, J.L. Jones, R. Ranjan, Anomalous reduction in domain wall displacement at the morphotropic phase boundary of the piezoelectric alloy system PbTiO₃-BiScO₃, *Phys. Rev. B* 93 (2016) 104103.
- [5] D.K. Khatua, K.V. Lalitha, C.M. Fancher, J.L. Jones, R. Ranjan, Coupled domain wall motion, lattice strain and phase transformation in morphotropic phase boundary composition of PbTiO₃-BiScO₃ piezoelectric ceramic, *J. Appl. Phys.* 120 (2016) 154104.

- [6] K.V. Lalitha, C.M. Fancher, J.L. Jones, R. Ranjan, Field induced domain switching as the origin of anomalous lattice strain along non-polar direction in rhombohedral $\text{BiScO}_3\text{-PbTiO}_3$ close to the morphotropic phase boundary, *Appl. Phys. Lett.* 107 (2015) 052901.
- [7] H. Liu, J. Chen, L. Fan, Y. Ren, Z. Pan, K.V. Lalitha, J. Rödel, X. Xing, Critical role of monoclinic polarization rotation in high-performance perovskite piezoelectric materials, *Phys. Rev. Lett.* 119 (2017) 017601.
- [8] J.L. Jones, E.B. Slamovich, K.J. Bowman, Domain texture distributions in tetragonal lead zirconate titanate by X-ray and neutron diffraction, *J. Appl. Phys.* 97 (2005) 034113.
- [9] A. Pramanick, D. Damjanovic, J.C. Nino, J.L. Jones, Subcoercive cyclic electrical loading of lead zirconate titanate ceramics I: Nonlinearities and losses in the converse piezoelectric effect, *J. Am. Ceram. Soc.* 92 (2009) 2291-2299.
- [10] A. Pramanick, D. Damjanovic, J.C. Nino, J.L. Jones, Origins of electro-mechanical coupling in polycrystalline ferroelectrics during subcoercive electrical loading, *J. Am. Ceram. Soc.* 94 (2011) 293-309.
- [11] G. Tutuncu, D. Damjanovic, J. Chen, J.L. Jones, Deaging and asymmetric energy landscapes in electrically biased ferroelectrics, *Phys. Rev. Lett.* 108 (2012) 177601.
- [12] J.L. Jones, E. Aksel, G. Tutuncu, T.M. Usher, J. Chen, X. Xing, A.J. Studer, Domain wall and interphase boundary motion in a two-phase morphotropic phase boundary ferroelectric: Frequency dispersion and contribution to piezoelectric and dielectric properties, *Phys. Rev. B* 86 (2012) 024104.
- [13] G. Tutuncu, L. Fan, J. Chen, X. Xing, J.L. Jones, Extensive domain wall motion and deaging resistance in morphotropic $0.55\text{Bi}(\text{Ni}_{1/2}\text{Ti}_{1/2})\text{O}_3\text{-}0.45\text{PbTiO}_3$ polycrystalline ferroelectrics, *Appl. Phys. Lett.* 104 (2014) 132907.
- [14] G. Tutuncu, J. Chen, L. Fan, C.M. Fancher, J.S. Forrester, J. Zhao, J.L. Jones, Domain wall and interphase boundary motion in $(1-x)\text{Bi}(\text{Mg}_{0.5}\text{Ti}_{0.5})\text{O}_3\text{-}x\text{PbTiO}_3$ near the morphotropic phase boundary, *J. Appl. Phys.* 120 (2016) 044103.
- [15] G. Tutuncu, B. Li, K. Bowman, J.L. Jones, Domain wall motion and electromechanical strain in lead-free piezoelectrics: insight from the model system $(1-x)\text{Ba}(\text{Zr}_{0.2}\text{Ti}_{0.8})\text{O}_{3-x}(\text{Ba}_{0.7}\text{Ca}_{0.3})\text{TiO}_3$ using in situ high-energy X-ray diffraction during application of electric fields, *J. Appl. Phys.* 115 (2014) 144104.
- [16] H.X. Fu, R.E. Cohen, Polarization rotation mechanism for ultrahigh electromechanical response in single-crystal piezoelectrics, *Nature (London)* 403 (2000) 281-283.
- [17] R. Theissmann, L.A. Schmitt, J. Kling, R. Schierholz, K.A. Schönau, H. Fuess, M. Knapp, H. Kungl, M.J. Hoffmann, Nanodomains in morphotropic lead zirconate titanate ceramics: On the origin of the strong piezoelectric effect, *J. Appl. Phys.* 102 (2007) 024111.
- [18] L. Rayleigh, Notes on electricity and magnetism, *Philos. Mag. Ser.* 23 (1887) 225-245.

- [19] D. Damjanovic, M. Demartin, H.S. Shulman, M. Testorf, N. Setter, Instabilities in the piezoelectric properties of ferroelectric ceramics, *Sens. Actuators A-Phys.* 53 (1996) 353-360.
- [20] R.E. Eitel, T.R. Shrout, C.A. Randall, Nonlinear contributions to the dielectric permittivity and converse piezoelectric coefficient in piezoelectric ceramics, *J. Appl. Phys.* 99 (2006) 124110.
- [21] D.A. Hall, Review: Nonlinearity in piezoelectric ceramics, *J. Mater. Sci.* 36 (2001) 4575-4601.
- [22] J.F. Nye, *Physical Properties of Crystals: Their Representation by Tensors and Matrices*. Oxford University Press, New York, 2000, p. 340.
- [23] D. Damjanovic, M. Demartin, The Rayleigh Law in piezoelectric ceramics, *J. Phys. D-Appl. Phys.* 29 (1996) 2057-2060.
- [24] V.D. Kugel, L.E. Cross, Behavior of soft piezoelectric ceramics under high sinusoidal electric fields, *J. Appl. Phys.* 84 (1998) 2815-2830.
- [25] Y. Zhang, D.C. Lupascu, Nonlinearity and fatigue in ferroelectric lead zirconate titanate, *J. Appl. Phys.* 100 (2006) 054109.
- [26] J.E. Garcia, R. Perez, D.A. Ochoa, A. Albareda, M.H. Lente, J.A. Eiras, Evaluation of domain wall motion in lead zirconate titanate ceramics by nonlinear response measurements, *J. Appl. Phys.* 103 (2008) 054108.
- [27] J.E. Daniels, A. Pramanick, J.L. Jones, Time-resolved characterization of ferroelectrics using high-energy X-ray diffraction, *IEEE Trans. Ultrason. Ferroelect. Freq. Control* 56 (2009) 1539-1545.
- [28] J.E. Daniels, J.L. Jones, T.R. Finlayson, Characterization of domain structures from diffraction profiles in tetragonal ferroelastic ceramics, *J. Phys. D, Appl. Phys.* 39 (2006) 5294-5299.
- [29] A. C. Larson and R. B. Von Dreele, *General Structure Analysis System (GSAS)*, Los Alamos National Laboratory Report LAUR 86-748 (2004).
- [30] J.L. Jones, M. Hoffman, K.J. Bowman, Saturated domain switching textures and strains in ferroelastic ceramics, *J. Appl. Phys.* 98 (2005) 024115.
- [31] D.A. Hall, A. Steuwer, B. Cherdhirunkorn, P.J. Withers, T. Mori, Micromechanics of residual stress and texture development due to poling in polycrystalline ferroelectric ceramics, *J. Mech. Phys. Solids* 53 (2005) 249.
- [32] D.A. Hall, A. Steuwer, B. Cherdhirunkorn, T. Mori, P.J. Withers, A high energy synchrotron x-ray study of crystallographic texture and lattice strain in soft lead zirconate titanate ceramics, *J. Appl. Phys.* 96 (2004) 4245.
- [33] D. Damjanovic, Contributions to the piezoelectric effect in ferroelectric single crystals and ceramics, *J. Am. Ceram. Soc.* 88 (2005) 2663.

- [34] M. Davis, M. Budimir, D. Damjanovic, N. Setter, Rotator and extender ferroelectrics: Importance of the shear coefficient to the piezoelectric properties of domain-engineered crystals and ceramics, *J. Appl. Phys.* 101 (2007) 054112.
- [35] J.L. Jones, A. Pramanick, J.C. Nino, S.M. Motahari, E. Ustundag, M.R. Daymond, E.C. Oliver, Time-resolved and orientation-dependent electric-field-induced strains in lead zirconate titanate ceramics, *Appl. Phys. Lett.* 90 (2007) 172909.
- [36] L. Fan, J. Chen, Y. Ren, Z. Pan, L. Zhang, X. Xing, Unique Piezoelectric Properties of the Monoclinic Phase in $\text{Pb}(\text{Zr};\text{Ti})\text{O}_3$ Ceramics: Large Lattice Strain and Negligible Domain Switching, *Phys. Rev. Lett.* 116 (2016) 027601.
- [37] J.L. Jones, M. Hoffman, J.E. Daniels, A.J. Studer, Direct measurement of the domain switching contribution to the dynamic piezoelectric response in ferroelectric ceramics, *Appl. Phys. Lett.* 89 (2006) 092901.
- [38] V. Mueller, Q.M. Zhang, Nonlinearity and scaling behavior in donor-doped lead zirconate titanate piezoceramic, *Appl. Phys. Lett.* 72 (1998) 2692.
- [39] D.V. Taylor, D. Damjanovic, Domain wall pinning contribution to the nonlinear dielectric permittivity in $\text{Pb}(\text{Zr};\text{Ti})\text{O}_3$ thin films, *Appl. Phys. Lett.* 73 (1998) 2045.

Figures

Fig. 1. Representative strain measurements at progressively increasing subcoercive electric field amplitudes up to 1.85 kV/mm at 0.33 Hz. A linear fit to the strain response yields the longitudinal piezoelectric coefficients. The error in strain determined from two samples of the same composition is less than 10%.

Fig. 2. Diffracted intensities of $\{002\}_{PC}$ (a) and $\{111\}_{PC}$ (b) diffraction profiles parallel to the electric field amplitude during application of a bipolar triangular wave (c). (d) Diffraction line profiles at 0 and 3.6 kV/mm.

Fig. 3. Calculated degree of domain orientation, $f_{002} = 3 \cdot (1/3 + \eta_{002})$ using multiples of random distribution (m.r.d.) unit and equivalent η_{002} values as a function of applied field amplitudes, during poling of the sample. 90° , 60° , 45° , 30° , and 0° represent the angles from electric field direction.

Fig. 4. Strain evolution in 111 reflection as a function of applied field amplitudes, during poling of the sample. 90° , 60° , 45° , 30° , and 0° represent the angles from electric field direction.

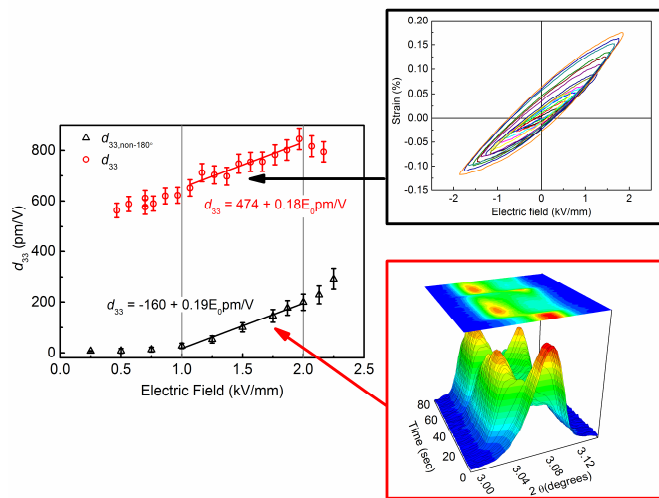
Fig. 5. (a) Contour plot of diffraction intensities of $\{002\}$ diffraction profile (T: tetragonal and M: monoclinic) parallel to the electric field amplitude during application of a square bipolar electric field of 1.5 kV/mm and frequency 0.33 Hz. (b) An example of the XRD pattern (symbols) and peak fitting (lines) corresponding to positive and negative segments of an applied field cycle measured parallel to the direction of the applied electric field. The difference between the two modeled profiles (i.e., acquired under positive vs. negative field) is shown at the bottom of the figure as a difference plot.

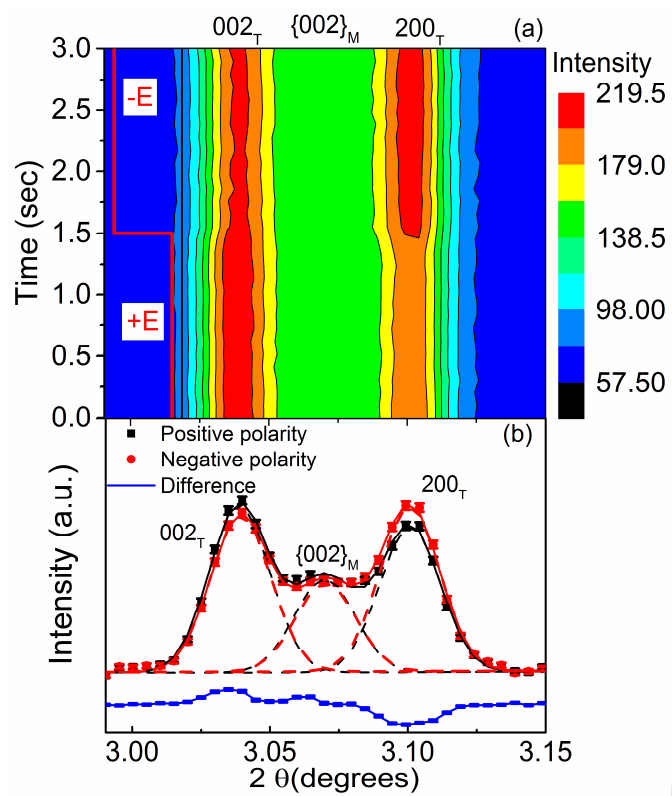
Fig. 6. Values of $\Delta\eta_{002}$ as a function of the angle from the applied electric field direction for

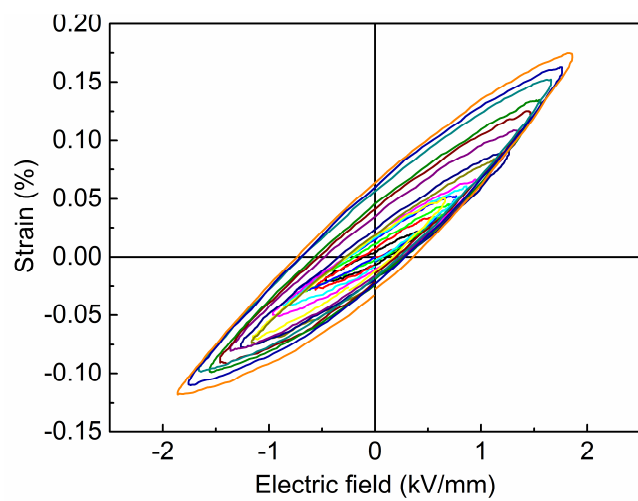
various field amplitudes. These values are calculated from the measured intensity interchanges of $\{002\}_{\text{PC}}$ reflections.

Fig. 7. Contribution of non-180° domain wall motion to the macroscopic strain coefficient, $d_{33 \text{ non-180}^\circ}$, calculated from the diffraction data and piezoelectric coefficient d_{33} values as a function of applied field amplitude, $\pm E$. Linear fits to these datasets in the linear region are shown as a solid line.

ACCEPTED MANUSCRIPT







ACCEPTED MANUSCRIPT

